The Taiwan-Ryukyu subduction-collision complex: Folding of a viscoelastic slab and the double seismic zone

Han-Chiang Chou,[1,2] Ban-Yuan Kuo,[3] Shu-Huei Hung,[1] Ling-Yun Chiao,[4] Dapeng Zhao,[5] and Yih-Min Wu[1]

Received 5 May 2005; revised 14 October 2005; accepted 22 December 2005; published 20 April 2006.

[1] The termination of the Ryukyu trench against Eurasia and the oblique subduction of the Philippine Sea plate create a subduction-collision complex offshore Taiwan, which has not previously been elucidated in detail. We combine traveltime data from the seismic networks in Taiwan and Japan to better illuminate how the subducting Ryukyu slab deforms in this subduction-collision zone. More than 5000 events recorded by both networks were relocated with the double-difference method using an optimal regional one-dimensional velocity model. The offshore seismicity indicates that the double seismic zone, with a gap of 15–20 km, exists in the subducting slab in the depth range of 40–80 km. Focal mechanisms suggest that the double seismic zone is caused by east-west compression resulting from oblique convergence. The improved hypocentral locations for the first time reveal folding of the slab into a horizontal curvature larger in magnitude than and opposite in sign to that of the Ryukyu trench in the depth range 50–100 km. The anomalous curvature, together with the focal mechanisms, suggests that the slab folds against the Eurasian lithosphere and that this deformation cannot be fully elastic. We model this deformation mode as the developing instability of a viscoelastic Maxwell layer embedded in a viscous medium. The characteristic wavelength of the instability, i.e., $\sim$250 km, is consistent with folding of a slab whose viscosity is 100 times higher than that of the surrounding mantle for an along-strike elastic membrane strain as small as 0.01, or more than 3 orders of magnitude higher if 5% elastic strain is allowed.

Citation: Chou, H.-C., B.-Y. Kuo, S.-H. Hung, L.-Y. Chiao, D. Zhao, and Y.-M. Wu (2006), The Taiwan-Ryukyu subduction-collision complex: Folding of a viscoelastic slab and the double seismic zone, *J. Geophys. Res.*, *111*, B04410, doi:10.1029/2005JB003822.

1. Introduction

[2] The global seismicity distribution provides a three-dimensional (3-D) portrait of each subduction zone in the mantle [e.g., *Chiu et al.*, 1991; *Engdahl et al.*, 1998]. These images demonstrate that the subducting slab largely inherits the geometric characteristics of the oceanic lithosphere formed on the surface of the Earth and tends to avoid additional extensibility or in-plane deformation [*Burbach and Frohlich*, 1986; *Yamaoka et al.*, 1986]. This implies that for a slab thousands of kilometers in lateral dimension but only tens of kilometers in thickness, the preferred mode of deformation is flexure instead of in-plane deformation. However, there are suggestions that flexure and large membrane deformation may occur simultaneously on regional to local scales in subducting slabs [e.g., *Bevis*, 1988]. In effect, the flexure mode of deformation produces changes in dip angle and/or the subducting flow field of the slab [*Chiao*, 1993]. Changes in the boundary forces that exert on the slab, such as the variations in the rates of trench migration and the impedance of the transition zone to deep penetration also distort the slab in three dimensions, introducing additional curvature to the slab geometry [e.g., *van der Hilst and Seno*, 1993; *Chen and Brudzinski*, 2001; *Pysklywec et al.*, 2003]. These deformations, however, are many hundreds to even thousands of kilometer along the strike of the trench, which can adequately be depicted using the seismicity data determined by the global network [*Gudmundsson and Sambridge*, 1998; *Engdahl et al.*, 1998].

[3] Several factors have to be in place favorably for the subducting slab to deform on scales of a few hundred km or less along its strike in the shallow mantle. The applied forces in the mantle have to be relatively localized or exerting on the slab in such a way to promote small-scale flexure. The rigidity of the slab sets a lower bound for the flexural wavelengths, so a thinner and warmer slab is prone to deflection than a stronger, older slab. The yield envelope governed by both friction and power laws [e.g., *Kohlstedt et al.*, 1995] delimits stresses in the slab, allowing for larger

[1]Institute of Geosciences, National Taiwan University, Taipei, Taiwan.
[2]National Cing Shuei Senior High School, Taichung, Taiwan.
[3]Institute of Earth Sciences, Academia Sinica, Taipei, Taiwan.
[4]Institute of Oceanography, National Taiwan University, Taipei, Taiwan.
[5]Geodynamic Research Center, Ehime University, Matsuyama, Japan.

0148-0227/06/2005JB003822$09.00

curvature for the same bending moment. Finally, the seismic data have to be accurate enough to characterize the deformation within hundreds of km in scale. Global seismicity data are likely to be aliased by limitations from the magnitude threshold of events and the global velocity model that are used, and are not up to the task. There are potential regions in which slabs are soft and subject to tectonic forces that may cause small-wavelength deformation but the global seismicity data fall short of resolving it.

[4] This study focuses on one of such potential regions: the westernmost 100 km of the Ryukyu subduction zone where the trench terminates against the Taiwan island at the surface and the slab against the Eurasian lithosphere at depths. Because of the increasingly high obliquity of subduction and the juxtaposing of the Eurasian lithosphere sideways, subduction is progressively superimposed with collision. In this relay zone northeast of Taiwan, the complex seafloor morphology and sediments obscure how the trench curves toward its western end, leaving no clue to project the shape of the slab below. Up-to-date, depiction of the slab in this region has been conducted with great limitations. Attempts based on the seismicity extracted from the global data set [*Engdahl et al.*, 1998] portray smooth, featureless structure [e.g., *Lin et al.*, 2004]. Because the zone is almost entirely offshore the island, use of the land-based network data risks systematic mislocation. From the geometrical viewpoint, several stations of the Japan network located on the westernmost islands of the Ryukyu arc provide a crucial constraint from the east of the relay zone. Unfortunately, joint seismological efforts between the two networks have not been realized to their full capacity in the past. It remains question as to whether the slab keeps intact in geometry as portrayed by previous studies when it edges toward the Eurasia.

[5] We combine data from Taiwan and Japan networks to relocate earthquakes in the 150-km-wide subduction-collision relay zone. The relocation process consists of necessary steps to assure minimum bias from either networks and to suppress the effects of three-dimensional heterogeneity. From the better determined seismicity in this study, a double seismic zone (DSZ) has been identified at intermediate depths throughout the onshore-offshore region, indicating that the DSZ imaged by *Kao and Rau* [1999] beneath the northern Taiwan extends eastward by at least 100 km. In addition, we observe a mild yet systematic deviation of slab geometry from that projected from the Ryukyu trench, and from that drawn previously based on either the global data set or the data of the Taiwan network [*Kao et al.*, 1998; *Hsu*, 2001]. Different modes of deformation in the relay zone may exist. In a kinematic consideration, *Chiao et al.* [2001] proposed an eastward rotation of subduction flow field to release the along-arc strain. While this rotation mode may exist, we establish a folding mode through the high-resolution slab geometry. We formulate an instability problem in which a viscoelastic layer is subject to compression to interpret under what rheological regime the folds take up the shape depicted by the relocated seismicity.

2. Taiwan-Ryukyu Subduction-Collision Complex

[6] The Ryukyu subduction zone has intimately engaged in the tectonic evolution of the northern segment of the Taiwan orogenic belt [e.g., *Sibuet et al.*, 1998] (Figure 1). Evolution of the volcanism both offshore and on land in the northern Taiwan is complicated but is ultimately derived from the back-arc spreading and upwelling in the mantle wedge behind the Ryukyu arc [*Wang et al.*, 2004a]. The mantle wedge beneath the western Ryukyu has not been imaged properly because of the poor coverage of seismic stations, except perhaps for the northern Taiwan where on-land seismic stations make such imaging geometrically possible [*Lin et al.*, 2004]. It is generally believed that the Okinawa Trough, the back-arc basin of the subduction system, extends into the northeastern corner of Taiwan, exerting a local extensional tectonism to the collisional regime of orogeny. The curvature of the trench has a maximum magnitude at the central segment on the order of 0.002 km^{-1}, on the same order of the magnitude of 0.001 km^{-1} of the Mariana. The small curvature throughout much of the trench favors a largely two-dimensional structure without significant along-strike deformation. The Philippine Sea plate (PSP) converges with the Eurasia at about 70 mm/yr along N50°W direction in this region (Figure 1) [*Seno et al.*, 1993]. The convergence is at high angle to trench for the eastern half of the trench, and that angle progressively decreases toward the west. Within a few hundred kilometers nearshore Taiwan, the angle becomes less than 20°, which signals a significant change of regional stress field with respect to the slab. In this zone, horizontal compression prevails as suggested by earthquake focal mechanisms [*Kao et al.*, 1998], and collision becomes the major force that could reshape the slab.

[7] In this ~100-km-wide subduction-collision relay zone, a few key problems remain perplexing. The Gagua ridge apparently intrudes into the trench at about 123°E (Figure 1), and the slab on the west of the Gagua ridge plunges more steeply than on the east [e.g., *Deschamps et al.*, 2000]. The origin of the ridge and its interaction with the overriding plate during subduction have been investigated [*Deschamps et al.*, 1998; *Schnurle et al.*, 1998]. The age of the western Philippine basin is important to the estimation of the mechanical strength and thermal structure of the Ryukyu slab, but has not yet been settled. The age of 40 Ma is estimated from the plate reconstruction model of *Seno and Maruyama* [1984]. Aided by dating of the gabbro samples, *Deschamps et al.* [2000] proposed a much older (>100 Myr) age for the Huatung basin, the portion of the PSP between Taiwan and the Gagua ridge. However, because the subduction is not straight north, most of the Huatung basin is on the course of collision with Taiwan and will never be subducted under the Ryukyu trench unless the plate motions change dramatically in the future (Figure 1). For the slab geometry, both teleseismic seismicity [*Engdahl et al.*, 1998] and the local earthquakes located by the Central Weather Bureau (CWB) Seismic Network of Taiwan have been selected to depict the Ryukyu slab in previous studies [*Kao and Rau*, 1999; *Font et al.*, 1999]. The CWB hypocenters exhibit smooth slab geometry that is no different from an extrapolation of the slab from the east [e.g., *Kao et al.*, 1998]. The slab contours shown by *Font et al.* [1999] using CWB data may reflect either inaccurate hypocenters or topographic features rather than flexure of a mechanical lithosphere. As noted above, a joint determination of seismicity from networks of Taiwan and Japan is

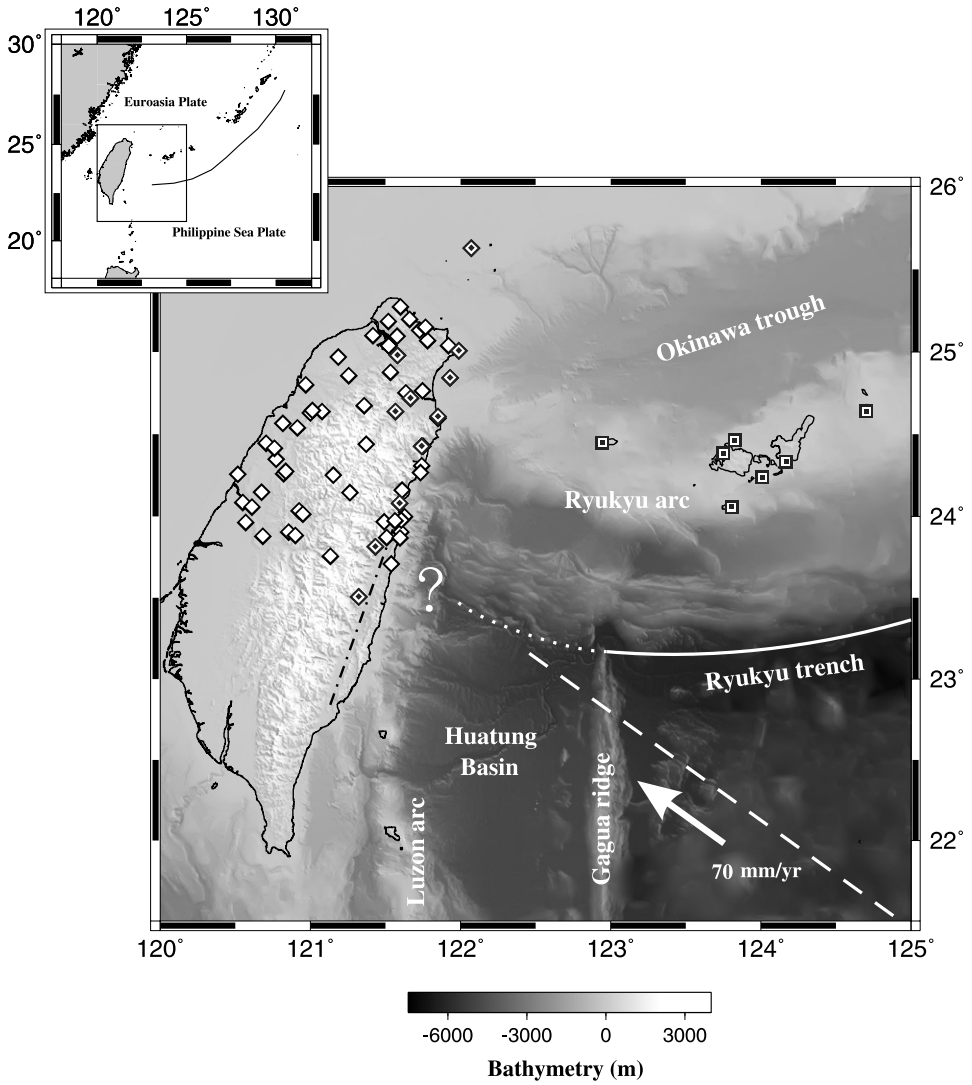

Figure 1. Map showing tectonic setting of the Taiwan-Ryukyu subduction-collision zone and the seismic stations used for relocation of earthquakes in this study. Major tectonic features are labeled. The 11 CWB stations (solid diamonds) and 7 JMA stations (solid squares) form a network covering the subduction-collision relay zone. For onshore events, the 11 CWB stations are joined by other CWB stations (open diamonds) to implement another network covering entire northern Taiwan. The Ryukyu trench has a general trend of southward convexity (white solid dotted line and black line in the inset) but loses its identification when nears Taiwan. Dashed line marks the hypothetical boundary, in the northeast of which the PSP will be subducted beneath the trench in the future. This boundary is parallel to the plate motion (arrow) [after *Seno et al.*, 1993]. The dash-dotted line running along the east coast of Taiwan marks the suture between the PSP and the Eurasia. Collision between the PSP and the Eurasian plate is taking place along this boundary and its northern extension in the upper mantle.

desirable. One of such attempt was made by *Hsu* [2001], which, with limited number of data from the Japan Meteorological Agency (JMA), represents a first step toward a comprehensive integration of data from the two networks.

[8] The crustal structure of the PSP at the forearc basin north of the trench has been investigated with multichannel/ocean bottom seismometry data by *Wang et al.* [2004b]. The resultant velocity model provides a glimpse of the physical state of the lithosphere at the onset of subduction. The 3-D velocity images show that the forearc basement warps in the arc-parallel direction, which is considered as evidence for buckling of the PSP lithosphere against the continental margin at Taiwan [*Wang et al.*, 2004b]. It is unknown whether this is a crustal signature or representative of the mechanical behavior of the entire PSP. In addition, the oceanic crust is thickened to ~10 km beneath the forearc in their model, but no further constraint exists at greater depths. Whether buckling or thickening persists in the subducting slab depends on whether the end barrier against the oblique subduction exists at greater depths and how the slab propagates flexure downward mechanically.

[9] *Kao and Rau* [1999] discussed the origin of the DSZ manifested in cross sections of CWB hypocenters onshore northern Taiwan, and recognized the horizontal compres-

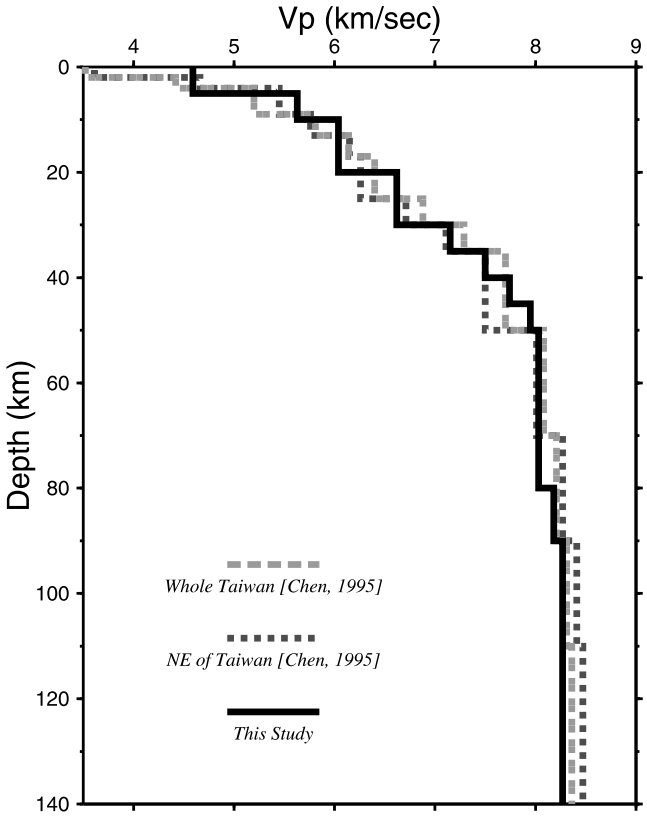

Figure 2. One-dimensional velocity model (solid line) determined by this study with the joint CWB-JMA data set and a manipulation to project the hypocenter effect away from the velocity determination. This model is used for the subsequent double-difference relocation. *Chen*'s [1995] subregional model for northeastern Taiwan is shown in comparison (dotted line). The similarity implies the dominance of slab structure in both.

sion as the tectonic stresses that are responsible for the double planed events. The authors interpret the formation of DSZ by drawing an analogy between oceanic slab and continental lithosphere, with the gap (defined to be 10–20 km) representing the ductile oceanic lower crust sandwiched between the brittle upper crust and upper mantle. The authors label it type II DSZ to distinguish it from those that have typically been associated with bending-unbending of the slab at greater depths, or type I. In this study, we identify DSZ throughout much of the offshore region, and analyze the pros and cons of both the "jelly sandwich" and the metamorphic reactions interpretations.

3. Data and Methods

[10] We first target more than 6000 earthquakes with magnitude greater than 4 that occurred during 1991–2003 initially located between 121.5 and 124.0°E and between 23.5 and 26.0°N. Eleven CWB stations near the northeast coast of Taiwan and seven westernmost stations of JMA were selected to geometrically bracket the relay zone (Figure 1). These earthquakes have been recorded by at least two CWB stations and two JMA stations to ensure a minimum level of even distribution of stations relative to events. The absolute arrival times were provided by the operators of both networks, and there are a total of 74,403 *P* and 60,952 *S* times to start with. Tomographic inversions have been conducted from the relocated events, and will be the subject of a separate report.

[11] The procedure of relocation is described below. The initial locations are taken from the CWB catalog, which is based on an average 1-D model of Taiwan determined by *Chen* [1995]. We then relocate these events using the combined CWB-JMA data and *Chen*'s [1995] subregional model for the northeastern Taiwan. To obtain a 1-D model that better represents the broader land-offshore region, we employ the technique of *Kissling et al.* [1994], which simultaneously inverts for the 1-D velocity structure and the hypocentral parameters, but to quench the latter using the projection operator method of *Pavlis and Booker* [1980] and only invert for the velocity model. The process decouples the velocity determination from the hypocentral effect, enhancing the independence of the former. The resultant 1-D model is shown in Figure 2. We do not use more in-land CWB stations for offshore events to avoid additional crustal heterogeneity in constructing our 1-D model for the relay zone. *Chen* [1995] also used the work by *Kissling et al.* [1994] for the CWB data but did not separate velocity from hypocentral effects. Her model for the northeast Taiwan is compared with our expanded land-offshore model in Figure 2. The discrepancy is not dramatic, implying that the deep structures of both models are dominated by the subducted PSP. Despite the fact that it is the case in the present study, we emphasize that it is always necessary to isolate the hypocentral effect from determination of the velocity model when secondary structures of the slab are pursued. Velocities below 150 km are relatively less well constrained in both models in Figure 2.

[12] We next use the double-difference method of *Waldhauser and Ellsworth* [2000] to relocate the hypocenters east of 121.5E using the 1-D model obtained above with the 11 CWB stations and 7 JMA stations. Then, we scan all the CWB events from 120.5 to 122°E to sort out those that are not relocated. These events include dropouts from the first round relocation due to lack of JMA constraint and new events that do not fall in the region for the first relocation, and are mostly onshore and well within the CWB network. They were then relocated using some 30 CWB stations in northern Taiwan, including the 11 stations in previous step (Figure 1). In this second round of relocation for mostly onshore events, we still use the velocity model specific for the offshore region to retain consistency in velocity model for the latter joint interpretation. Moreover, we are interested more in the subduction zone structure than the crust of Taiwan; as described below, the double-difference approach reduces the near station heterogeneity effects such that differences in shallow crustal velocity between models are not critical. Both rounds of double-difference relocation achieved greater than 70% variance reduction in differential traveltimes.

[13] The double-difference algorithm minimizes the residuals of the differential times between hypocentral pairs. It works efficiently for relative locations between multiplets, sparing the need for station corrections. We adopt it in this study to relocate regional earthquakes by minimizing the effect of crustal and mantle heterogeneities, in that the 3-D

velocity anomalies picked up by the Fresnel zone of each of the paired ray paths to a common station are suppressed by the differential times. The key parameter here is thus the radius, r_0, within which each event seeks to pair with neighboring events to form the differential times. In regional problems, r_0 should be set to correlate with the scale of heterogeneity relative to the Fresnel zone of the waves. It may risk higher chance of contamination from velocity heterogeneities if a larger value is used. Small r_0 ensures suppressed heterogeneity effect, but suffers from relocating events with limited number of differential times. For deeper events, the Fresnel zones of the paired path are less separated beneath the stations than for shallow events, allowing for a larger r_0. We focus on the slab structure and adopt $r_0 = 30$ km. Use of $r_0 = 20$ km does not produce different results because the average distance of pairing for each event is much smaller than r_0. The number of event pairing at the depth range of 50–150 km is several tens to over 100. The number drops to around 10 below 150 km. The maximum and minimum numbers of pairing in this study are set to be 100 and 8, respectively. Some deeper events are too isolated to have enough pair-wise observations, and have therefore been discarded. After the double-difference relocation, the number of events reduces to 5667 and the numbers of *P* and *S* arrivals to 69760 and 57412, respectively.

[14] The merit of the double-difference relocation in a 1-D velocity model versus the 3-D corrected, ''single'' difference approach for regional and teleseismic studies is debatable. The choice between the two lies in our confidence in the 3-D tomographic model used for the 3-D correction. While no difficulty in detecting the existence of the subducting slab convincingly, the tomographic inversions are usually highly underdetermined, and the result severely weighted and smoothed [e.g., *Ma et al.*, 1996; *Rau and Wu*, 1995]. Moreover, shallow structures in these tomographic models are loosely constrained. Recently, *Kim et al.* [2005] systematically evaluated the effects of station correction in imaging the crust of Taiwan. This model presents improved constraint on the shallow structure and consequently the crust below, which may serve as a starting model for 3-D earthquake locating. Offshore crust and upper mantle, however, are not covered in their study. On the basis of our experiences in earthquake relocation and 3-D tomographic inversion using the combined CWB and JMA data, we believe that the tomography-based 3-D correction is probably premature for the studied region despite it could be the ultimate goal. *Wu et al.* [2004] also used double-difference method to locate events throughout Taiwan to probe the internal structure of the orogen.

[15] In this paragraph we assess how different timing systems of the two networks may affect hypocentral locations. The records of the JMA stations used in this study are time tagged at the stations, while the CWB data are stamped with GPS times at the CWB data center after the data are telemetered from each station. It has been optimistically assumed that the delay due to telemetry is negligible, and therefore the magnitude of delay has not been quantified at least for stations in northern Taiwan. To examine its effect on our results, we analyze the differences in *P* arrival times recorded by two collocated stations, the CWB station NWF and the broadband station WFSB which employs local time tagging, for events in 1999–2004. Statistics of the *P* arrival differences shows a mean of 0.03 s and a standard deviation of 0.02 s. Because NWF and WFSB are the only collocating stations in northern Taiwan, we assume that this statistics is representative. We estimate whether delays of this amount throughout the network cause severe bias in locations when data of the two networks are merged. To do this, the CWB arrival times were shifted earlier by a random number that is characterized by a mean of 0.03 s and a standard deviation of 0.02 s before merging with the JMA times. The double-difference relocation was then performed with this test data set to obtain a new hypocenter distribution. This new distribution is very similar to the original one, and consequently both the geometry of the slab and the first-order seismogenic structures entertained in sections 4–6 remain the same. We conclude that the time-tagging process operated by CWB does not bias the hypocenters significantly with respect to the features concerned in the present study.

4. Results: Slab Geometry and Seismogenic Pattern

[16] Distribution of earthquakes is shown in a sequence of horizontal slices at various depths (Figure 3). The seismicity in the uppermost 20 km reflects stresses in the PSP lithosphere and the overriding Eurasian plate, and seems to bundle with the tectonic elements of the trench system. The trench-parallel pattern mirrors the morphological fabrics of the trench [cf. *Font et al.*, 2001, Figure 1]. In the Okinawa trough, shallow seismicity is aligned with the spreading axis of the back-arc basin that apparently juxtaposes against the northeastern coast of Taiwan (Figure 3, 0–15 km). Down from the depth of 50 km, the seismicity delineates the geometry of the subducting slab. To visualize how the slab deforms, we picked the northernmost events at each 10-km depth interval and 0.1° longitude interval to represent the upper boundary of the slab and form a 3-D data set. Obvious outliers are ruled out. The rationale behind this representation is the knowledge that events do occur in the crust of the slab, making them good proxy of the surface of the slab. We then fit this data set with a surface using the software GOCAD [*Mallet*, 1989, 2002]. GOCAD employs least squares fitting of points in 3-D to a surface under the regularization of minimum curvature and gradient. If seismic gaps exist in the data set, they will be filled by this regularization requirement. We also experimented a different way of representing the slab upper surface. Instead of taking the northernmost event in a narrow interval, the three northernmost events in each 0.25 longitude interval were averaged, and no ''outliers'' were removed before fitting with GOCAD. The two different approaches produce very similar slab geometry, and the result of the first is shown in 3-D perspectives in Figure 4.

[17] The depth contours of the GOCAD surface are also plotted with the epicenters in Figure 3 from 45 to 115 km depths to illustrate how plate flexes along its strike. Note the depth contour may not match exactly the seismicity boundary in each cross section because the fitting is constructed in 3-D which is a robust way to describe the slab surface compared with the 2-D fitting of earthquakes in each depth interval. At roughly 123°E, a group of events extrudes from the average strike of the slab in the vicinity, most likely

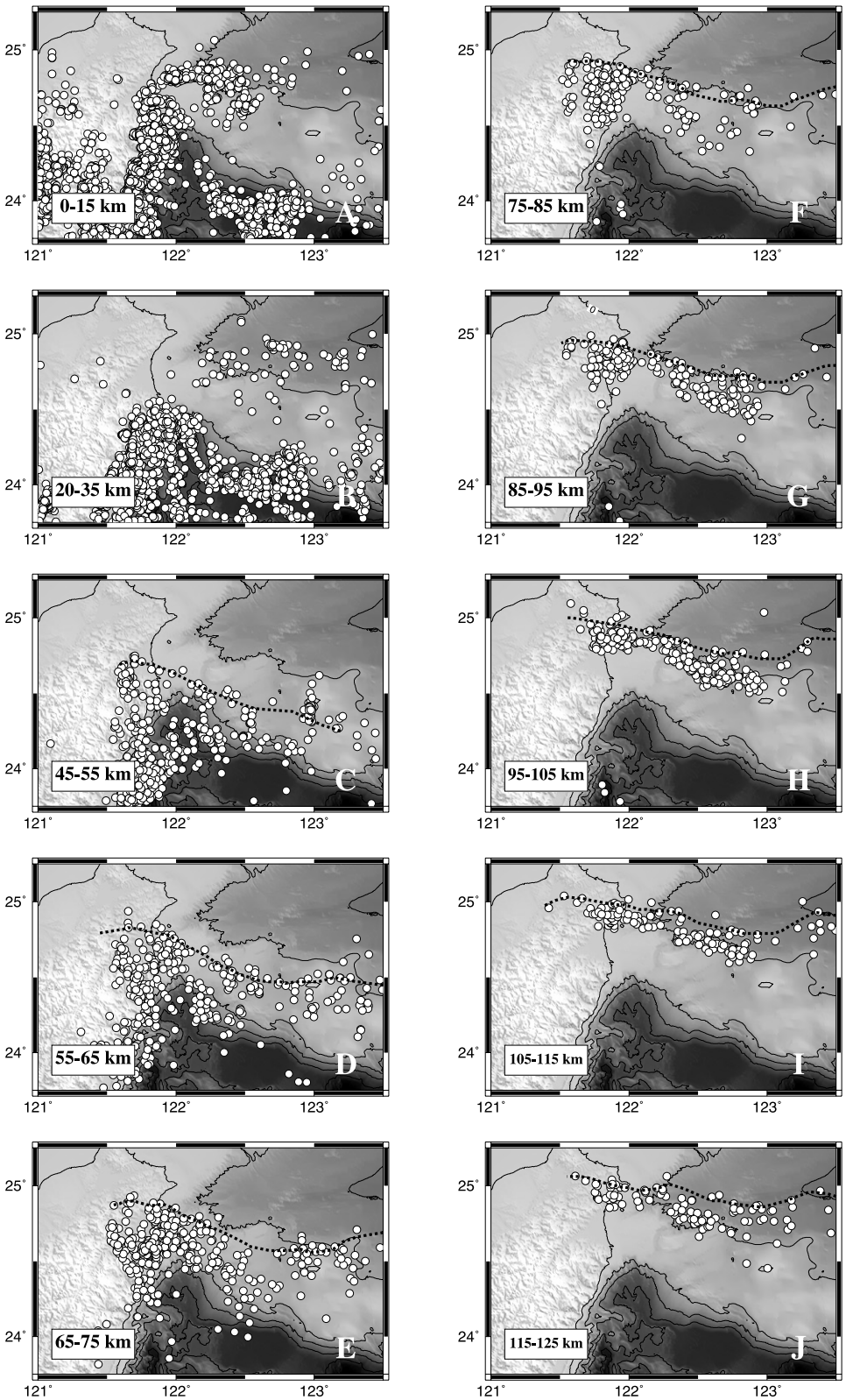

Figure 3. Depth slices showing relocated earthquakes (open dots), with the depth interval annotated. The depth contours (black dotted lines) are taken from the 3-D slab surface model in Figure 4 at the central depth of each interval. The slab contours generally follow the trend of the Ryukyu trench. Near the western boundary in the depth range 45–95 km, however, the slab shows a revered curvature with respect to the trench (C to G).

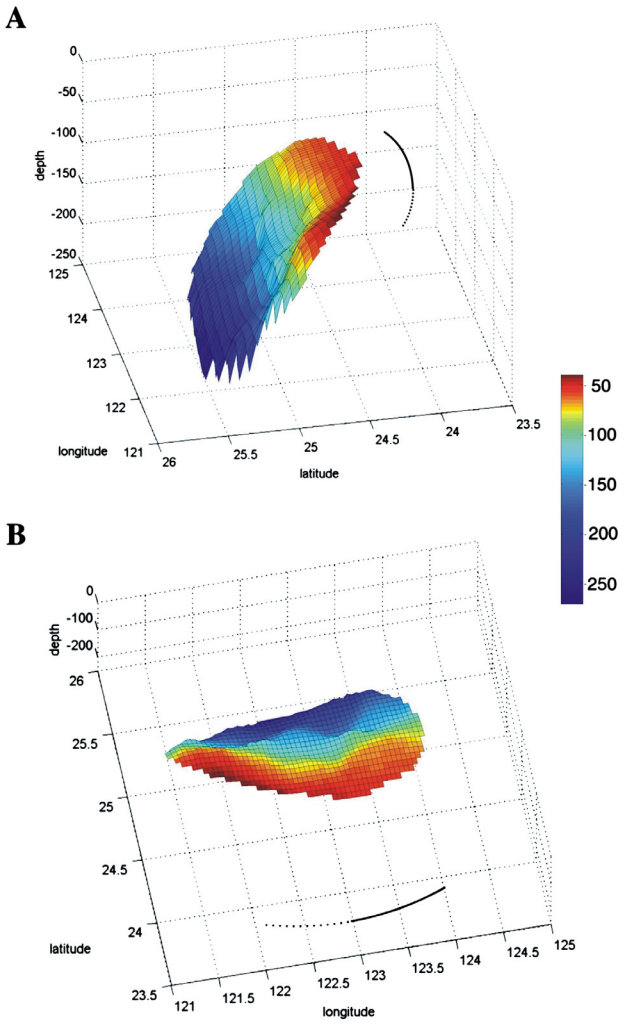

Figure 4. The 3-D slab surface model fit using GOCAD software, shown in two different perspectives. (a) From northwest to see the face of the slab. The folding over the western section creates a bulge at intermediate depths that leads to a greater dip angle of the slab below. (b) A look that grazes along the surface of the slab from south to north subparallel to the slab dip. In both Figures 4a and 4b, folding near the western boundary is evident in comparison with the trace of the trench (solid and dotted lines in Figures 4a and 4b).

representing a topographic structure such as a seamount or even part of the nearby Gagua ridge. The slab surface we determined apparently skips this seismic structure (e.g., Figure 3, 45–55 km). The contours are generally subparallel to the trench, except for the bend over in the westernmost 50 km over the 45- to 95-km depth range. This structure is significant in that it bends reversely with respect to the general trend of the Ryukyu trench (Figure 4).

[18] To examine whether this feature is robust, we add random errors of 5 km to both epicenter and focal depth of each earthquake and fit this "contaminated" data set using GOCAD with both schemes of representation. The bulge near the western end of the slab remains prominent in the new GOCAD surface. To falsely produce such bulge, the events in the westernmost 50 km over a few tens of kilometer depth range must be systematically displaced by 5–10 km toward south: a scenario considered unlikely under the tight constraint provided by the dense land stations in northern Taiwan. Although visually mild in both Figures 3 and 4, the bulge is characterized by an along-strike horizontal curvature κ_h of 0.02–0.04 km^{-1} at the peak of the bend over, much larger than the "background" curvature of 0 to -0.002 km^{-1} measured for the western 1/3 of the Ryukyu trench. As another reference, the curvature of the strongly curving Mariana trench in the vicinity of the midpoint along the strike has a magnitude of only 0.001 km^{-1}. The observed curvature for the western Ryukyu slab is significant not only for its magnitude but also for its opposite sign to that of the Ryukyu trench. As analyzed in section 5, its relatively short wavelength is also unique.

[19] The curvature is related to the elastic bending strain by $\varepsilon(z) = -(z - h/2) \cdot \kappa$, where z is depth from the top surface of the elastic plate with a thickness h. Taking the average κ measured normal to the slab dip to be 0.04 km^{-1} and a conservative h of 15 km, the strain at the upper surface of the plate $\varepsilon(0) = \sim 0.3$, which is too large for an elastic plate. Continual brittle failure allows for smaller elastic strain with apparently larger curvature, but the upper portion of the slab still experiences horizontal tension in this scenario, in contradiction with the focal mechanisms that show east-west oriented compression and a downdip tension for the slab [*Kao and Rau*, 1999; *Liang et al.*, 2004] (see below). This suggests that the slab in the westernmost Ryukyu subduction zone responds elastically only to the horizontal compression, rather than to the tension implied by the curvature. We advocate that the slab folds to a large extent viscously to form the bulge in horizontal sections, with a timescale independent of the compressional brittle failure. We return to this mechanism and explore under what condition it may work in section 5 with a viscoelastic formulation.

[20] Five vertical cross sections were taken in directions normal to the local strike of the slab in the depth range of 50–100 km and are shown in Figure 5. As far as the vertical profiles can discern (Figure 5), the slab kinks (vertically) between 50 and 80 km in profiles A, B, and C, and kinks at depths shallower than 40 km and straightens downdip from 50 to 150 km in profiles D and E. The 3-D model in Figure 4 shows that the bulging is a 3-D structure that is part of the fold of the slab seen in horizontal cross sections described in the preceding paragraphs. As a result, the dip of the slab below 80 km increases toward the west. In contrast to *Deschamps et al.* [2000], who report the average dip difference across the Gagua ridge, the relocated hypocenters resolve secondary variations in the dip of the slab west of the Gagua ridge.

[21] Another prominent feature about the Wadati-Benioff zone is the DSZ, which appears over most of the vertical sections in the relay zone. There are substantial along-strike variations in the DSZ configuration. The DSZ is more ambiguous on profile B than on other profiles where the DSZ depth extents are variable. The two planes appear to converge in profile C, but such convergence is not clear elsewhere. In general, the gap of the DSZ is 15–20 km wide from 40 to 80 km depths. The depth extend is short

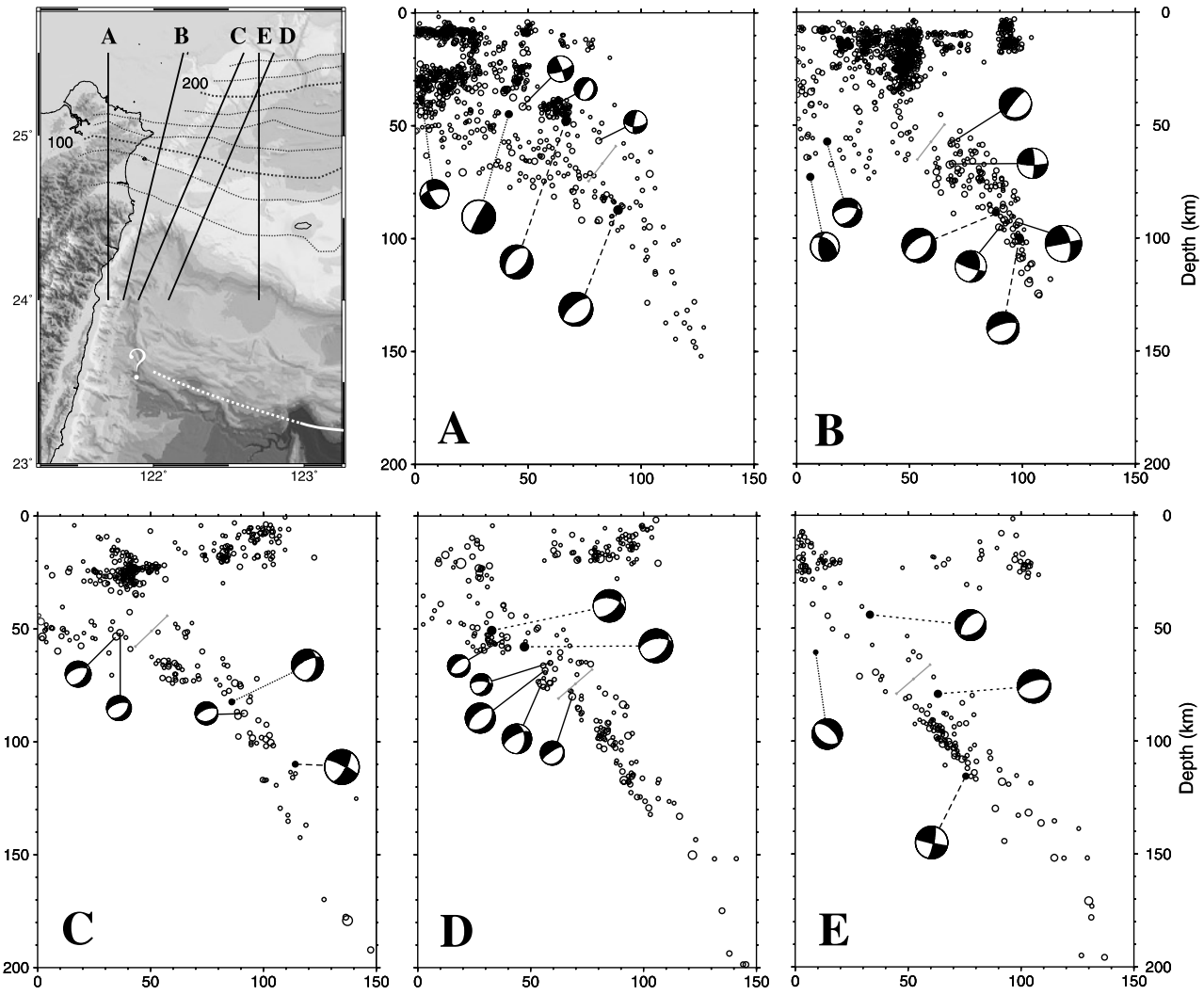

Figure 5. Wadati-Benioff zone in different vertical cross sections whose locations are shown in the upper left panel. Thin and thick dotted lines in black are depth contours of the slab surface taken from the 3-D model in Figure 4, and each profile is taken to be perpendicular to the strike of the slab at shallow depths (<100 km). White solid and dotted lines are traces of the Ryukyu trench the same as in Figure 1. In profiles A, B, and C, the slab apparently bends/unbends vertically between 50 and 80 km such that its dip below is increased relative to that in profiles D and E. The DSZ morphology varies substantially across profiles, but overall two planes are separated by 15–20 km, as indicated by the 20-km-long ruler with 10-km ticks. Side projection focal mechanisms from *Liang et al.* [2004] (solid line connection), *Kao and Rau* [1999] (dashed line), and the Harvard database (dotted line) show minor variation, with a consistent component of along-strike, east-west oriented compression between 50 and 100 km (the white quadrant contains *P* axis). The DSZ extends from onshore to offshore for at least 100 km.

compared with the DSZ in the subduction zone beneath the northeast Japan [*Hasegawa et al.*, 1994]. It is hard to distinguish which plane, the upper or the lower, terminates first and which plane continues downdip. The focal mechanisms determined by *Kao et al.* [1998], *Liang et al.* [2004], and the Harvard Centroid-Moment Tensor (CMT) [e.g., *Dziewonski et al.*, 1981] primarily show along-strike compression in both the upper and the lower plane of the DSZ, indicating that at least the brittle part of the subducting slab is subject to one consistent stress field. Departure from the along-strike compression exists, e.g., focal mechanisms in profiles A and B show coexistence of slab-parallel and slab-normal *P* axes, probably owing to local stress change where slab deforms significantly. Along-strike folding could relax the compression, causing a switch of compression axis from slab parallel to slab normal. Despite this, the overall pattern of focal mechanisms supports our assertion that the DSZ and the folding of the slab originate from the same horizontal compressive forces, and that folding develops mainly viscously.

5. Folding of the Slab

[22] Note from Figure 4 that the horizontal folding persists over about 50 km downdip, not an artifact fortuitously determined by a single profile at a particular depth.

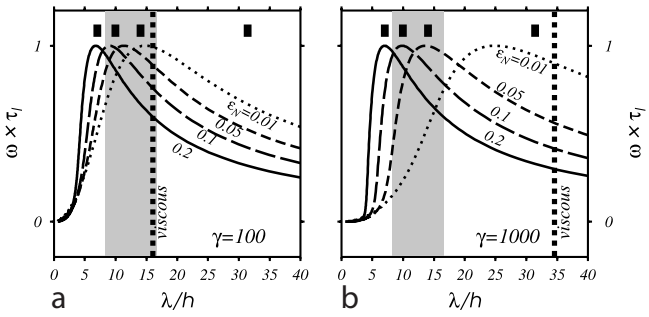

Figure 6. Predicted nondimensionalized amplification $\omega_1 \times \tau_l$ as a function of wavelength for (a) $\gamma = 100$ and (b) $\gamma = 1000$ and for the elastic strain $\varepsilon_N = 0.01$ (dotted lines), 0.05 (short dashed lines), 0.1 (long dashed lines), and 0.2 (solid lines). The amplification functions are normalized to 1. The dominant wavelength for a viscous layer (vertical dotted line) is a function of γ only, and is approximated by the viscoelastic layer at small ε_N. The dominant wavelength of an elastic buckling is a function of ε_N, indicated by the short vertical bars near the top of Figures 6a and 6b for $\varepsilon_N = 0.2$, 0.1, 0.05, and 0.01 from left to right. Pure viscous folding barely explains the observation (shaded region) with $\gamma = 100$ (or smaller), and a pure elastic slab requires strain >0.04. Both are inadequate in explaining the status of stress of the slab.

The earthquake mechanisms and magnitude of curvature suggest to us that the slab responds to the lateral compression elastically with brittle failure but viscously to develop large curvature. The former is characterized by a timescale of seconds and the latter by a much longer timescale on the order of hundred thousands to millions of years. We simulate this deformation scenario as a viscoelastic layer embedded in a viscous medium, in that folding results from instability that grows most efficiently at particular wavelengths controlled by the rheology contrast between the layer and the medium as well as the magnitude of the elastic shortening or membrane strain. The critical constraint is thus the wavelength of the dominant member of the fold, λ_d. A spectrum analysis of the slab contours in the corresponding depth range yields $\lambda_d \sim 250$ km. We could as well estimate $\lambda_d/2$ by measuring the distance between the peak of the fold (near the western end) and the "background," or $\lambda_d/4$ by the distance between the peak and the inflection point where $\kappa = 0$. The results are mutually consistent, indicating that the estimate of 250 km is robust. We derive the governing equation of flexure of a thin Maxwell-type viscoelastic layer and the associated instability problem in Appendix A. The flexure equation reads

$$D_v \frac{\partial w''''}{\partial t} + N w'' + \tau_l N \frac{\partial w''}{\partial t} = -4k\mu_m \frac{\partial w}{\partial t} - 4k\mu_m \tau_l \frac{\partial^2 w}{\partial t^2}, \quad (1)$$

where w is the deflection of the layer, t is the time, w'''' denotes $\partial w^4/\partial x^4$, and so forth with x parallel to the layer, N the x-parallel horizontal compressive force per unit perpendicular to x, D_v the viscous rigidity of the layer, τ_l the relaxation time of the flexure of the Maxwell layer, μ_m the viscosity of the medium or the upper mantle, and k the wave number of flexure and of the viscous resistance of the medium. Other parameters are explained in Appendix A.

[23] Following the derivations laid out in Appendix A, it is shown that a Maxwell layer has two components of instability during folding each characterized by an exponential function of time: $\exp(\omega_1 \cdot t)$ with $\omega_1 > 0$, which is unstable and will amplify with time, and $\exp(\omega_2 \cdot t)$ with $\omega_2 < 0$, which is stable and will eventually die out. The amplification $\omega_{1,2}$ is function of the ratio of the viscosity of the layer to the viscosity of the medium $\gamma = \mu_l/\mu_m$, the equivalent elastic membrane strain $\varepsilon_N = N/(E_l^* h)$ (see Appendix A), and the wave number of each fold member k (or wavelength λ). Because we assume that the observed large-amplitude folding results from instability, we focus on ω_1 as a function of wavelength. The nondimensional amplification $\omega_1 \cdot \tau_l$ versus λ/h is shown in Figures 6a and 6b for different values of γ and ε_N. The peak of the amplification function marks the model dominant wavelength λ_d^{obs}/h at which folding preferentially grows.

[24] To establish the observed dominant wavelength λ_d^{obs}/h as the target for modeling, we need to estimate h. Because the gap of the DSZ is 15–20 km, the seismogenic thickness of the slab is probably greater than 20 km (Figure 5). However, h represents the effective mechanical thickness of the viscoelastic layer, and usually is smaller than the seismogenic thickness of the lithosphere [*Cochran*, 1979; *Wiens and Stein*, 1984]. Combined analyses of gravity and topography and mechanical modeling of oceanic lithosphere in the past have indicated that the effective elastic thickness of the oceanic lithosphere ranges from <10 km near mid-ocean ridge [*Cochran*, 1979; *Kuo et al.*, 1986] to 20–30 km in old oceanic basins [*Caldwell et al.*, 1976; *Watts*, 1978]. We assume the lower bound of h to be 15 km, partially reflecting the fact that the slab is heated relative to the lithosphere before subduction, and set the upper bound at 30 km. The range of λ_d^{obs}/h is 8.3–16.7 (Figure 6).

[25] Figure 6 compares models with observations. Because stronger compression is required to fold a more viscous layer, ε_N has to be large for larger γ, and vice versa, to keep λ_d^{mod}/h within the observation domain. Larger ε_N can also be achieved with larger N, smaller h, and lower Young's modulus, but neither of these is under sufficiently tight geophysical constraints. However, the strain is limited by the yield envelope of the slab in the presence of earthquakes. For the compressional yield strength on the order of 500 MPa given by the friction law for the oceanic lithosphere at tens of km depth [e.g., *Kohlstedt et al.*, 1995] and a commonly accepted Young's modulus range of 10^{10}–10^{11} Pa, the elastic strain could range from very small to 0.05. We consider 0.05 the ad hoc maximum of ε_N. It is unlikely that the viscosity of the subducting slab approaches that of the shallow upper mantle as long as the slab continues to plunge without disintegration or strong folding. We assume $\gamma \geq 10$, which, as shown below, is overridden by the lower bound of λ_d^{obs}/h. Permissible set of model parameters may be found in the $\gamma - \varepsilon_N$ diagram

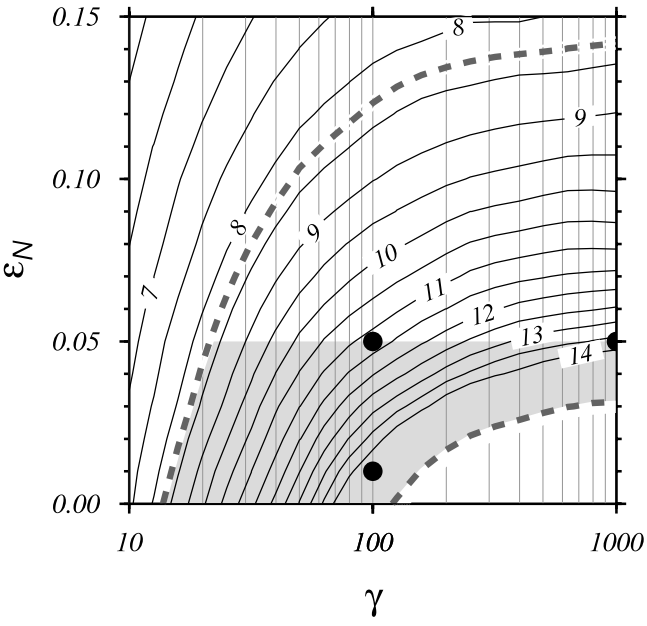

Figure 7. Possible parameter regime of the Maxwell viscoelastic model entertained in this study. Solid contours are model dominant wavelengths nondimensionalized by thickness. The regime (shaded) is delimited by the possible maximum elastic strain ε_N of 0.05 and possible bounds of the observed wavelengths at 8.3 and 16.7 (dashed lines). Higher strains allow for a wide range of viscosity contrast between slab and upper mantle, while for smaller strains only small values of γ are acceptable. Solutions discussed in the text, i.e., $\gamma = 100$, $\varepsilon_N = 0.01$ and 0.05 and $\gamma = 1000$, $\varepsilon_N = 0.05$, are marked by solid squares. Future independent constraints on either parameter will help narrow the permissible model regime.

bounded by $\lambda_d^{obs}/h = 8.3$ and 16.7 and $\varepsilon_N = 0.05$ (Figure 7). As an example, a slab with a viscosity 100 times higher than that of the upper mantle and a 5% horizontal elastic strain is able to fold into a dominant wavelength of 250 km if the effective thickness is slightly greater than ~22 km ($\lambda_d^{obs}/h \sim 11.4$).

[26] Can pure elastic or viscous folding explain the observed dominant wavelength? The Maxwell layer can be reduced to an elastic layer by setting $\tau_l \rightarrow \infty$ (see Appendix A), for which the dominant wavelength of instability decreases as ε_N increases (Figure 6). For the same ε_N, elastic layer predicts broader folds than the Maxwell layer. To buckle an elastic plate into the observed wavelength, ε_N has to be 0.04 or greater. While this is acceptable, elastic buckling is not appealing on the ground that the tensional bending strain it produces contradicts the earthquake mechanisms that show overall compression throughout the thickness of the slab. On the other hand, a viscous layer is obtained when $\tau_l = 0$. The dominant wavelengths in this case approximate the Maxwell folding with small ε_N (Figure 6). This implies that the elastic component in the form of horizontal shortening of the slab assists in developing shorter-wavelength folds. The viscous folding is favorable only for smaller values of γ (Figure 6a), and again it fails to incorporate the elasticity to properly account for the intraslab earthquakes and their compressional focal mechanisms.

6. Discussion

[27] We cannot further narrow the permissible regime of model parameters because the viscoelastic formulation is a simplified approach as well as knowledge of model parameters has been fuzzy. Instead, we choose to draw a broader acceptable model regime in order to explore the tradeoff effect between γ and ε_N and keep the issue open until new independent constraints are available. For a strong slab that is >3 order of magnitude more viscous than the mantle, the in-plane elastic strain ε_N has to be at least 0.04 to explain the observed wavelength (Figure 7). For a weaker slab or lower γ, a wide range of strain is allowed due to the poorly known h. The γ of 100 is considered near the low end of the spectrum [*Houseman and Gubbins*, 1997; *King*, 2001; *Billen et al.*, 2003]. A rule of thumb based on dynamic modeling of Newtonian fluid and power law viscosity is 100°C decrease in temperature leading to roughly 0.5–1 order of magnitude increase in viscosity at mantle temperatures [e.g., *Christensen*, 1989; *Lin et al.*, 2002]. A γ of 100 implies an average temperature contrast of 200°C for Newtonian and 400°C for non-Newtonian fluids. An average temperature anomaly of 200°C is probably hard to reconcile the thermal model for the Ryukyu subduction zone constructed by *Yamasaki and Seno* [2003]. While 400°C seems acceptable, the corresponding non-Newtonian dynamic effect for a subduction zone is not fully understood yet. Perhaps ε_N is the parameter on which constraints may be improved in the future. Estimation of the elastic strain the slab is experiencing from seismological point of view may be a useful step toward pinpointing a solution in our permissible model space [e.g., *Bevis*, 1988].

[28] The DSZ at intermediate depth range (40–150 km) have been observed in several subduction zones [e.g., *Hasegawa et al.*, 1978; *Abers*, 1992; *Kawakatsu*, 1986; *McGuire and Wiens*, 1995]. The upper plane seismicity is thought to occur in the oceanic crust and has been widely accepted to be associated with basalt-eclogite transformation [*Kirby et al.*, 1996; *Peacock and Wang*, 1999; *Peacock*, 2004]. A few hypotheses have been put forth on triggering mechanisms for the lower-plane seismicity [see *Yamasaki and Seno*, 2003], among which the dehydration embrittlement of the serpentinized slab mantle [*Seno and Yamanaka*, 1996; *Peacock*, 2001] suits the depth range discussed in this study. A global survey on the spatial correlation between these metamorphic reactions and the geometry of the DSZ is carried out by *Yamasaki and Seno* [2003]. In their cross sections beneath northern Taiwan, the correlation between the DSZ and the predicted dehydration loci is not clear, although the calculated gap of about 20 km between the two reaction loci matches our observation.

[29] It has been proposed that the serpentinization of the mantle can be made by infiltration of water along the large faults that rupture the upper portion of the lithosphere before subduction, usually on the outer rise [e.g., *Peacock*, 2001]. Tracing opposite the plate motion direction, the section of the PSP lithosphere that would be subducted to the current location of DSZ is to the southeast of the relay zone (Figure 1), where present-day large outer rise events

have been sparse. The only one documented in the Harvard CMT catalog is a M5.7 normal faulting event, which has a standardized centroid depth of 15 km and a source dimension of at most 10 km. Whether serpentinization of the slab interior can be facilitated by a few outer rise faults like this one remains in doubt. In the outer rise region of the Ryukyu trench, in situ imaging of lithosphere that could provide direct evidence for or against deep cutting faults [e.g., *Ranero et al.*, 2003] has not been conducted. Critical supportive evidence for dehydration embrittlement through faulting in this region remains lacking.

[30] *Kao and Rau* [1999] invoked a jelly-sandwich-type of rheology much like that of the continental lithosphere to explain the DSZ seismogenic pattern in the onshore region (see section 2). While rheology of oceanic lithosphere may be potentially important [e.g., *Wang and Rogers*, 1994], drawing analogy between continental and oceanic lithosphere is risky. The ductility of the oceanic lower crust has been under debate [*Kohlstedt et al.*, 1995; *Escartin et al.*, 1997; *Hirth et al.*, 1998]. It is common that microearthquakes as well as earthquakes with magnitude up to 4 nucleate at lower crustal depths along and near mid-oceanic ridges [e.g., *Wolfe et al.*, 1995; *Bergman and Solomon*, 1990]. Most importantly, at the depth below 40–50 km, where the DSZ in this study is best identified, high lithostatic pressure prohibits brittle failure if unassisted by elevated pore pressures [e.g., *Kirby*, 1995]. In southern Cascadia where the rheology interpretation was originally put forth for subducting slab [*Wang and Rogers*, 1994], the DSZ is distributed in a much shallower depth range (10–25 km). Another uncertain factor is the thickness of the oceanic crust. In this study, the gap of 15–20 km would, in *Kao and Rau*'s [1999] scenario, represent an oceanic crust 2 or 3 times thicker than normal (~7 km) over a large area on the slab. Up-to-date seismological evidence from the PSP has not been convincing in favor of a much thickened crust of PSP [*Wang et al.*, 2004b]. Thickening the crust magmatically or mechanically by a factor of 2 or 3 is considered less likely to occur. In contrast, the two layers found in southern Cascadia subduction zone are separated by less than 10 km [*Wang and Rogers*, 1994]. Speculations over the origin of the DSZ in the Taiwan-Ryukyu collisional zone should defer until more solid evidence becomes available.

7. Conclusions

[31] Accurately determined 3-D seismicity prompts us to reinterpret the deformation of the Ryukyu slab with better kinematic constraints. The seismicity distribution for the first time reveals folding of the slab in the along-strike direction at the depth range of 50–100 km. The folding is significant in two ways: its curvature is greater in magnitude than and opposite in sign to that of the Ryukyu trench, and its wavelength is relatively short at ~250 km. It suggests that the folding results from the horizontal compression exerting on the slab by the resistance of the Eurasian lithosphere against the oblique subduction of the PSP. Both the focal mechanisms and the large curvature argue in favor of a folding generated by viscoelastic instability. We envision a deformation scenario in which the slab responds to the compression through both brittle failure and viscoelastic folding against the Eurasian lithosphere. A Maxwell-type model is employed to simulate this scenario, and to help constrain acceptable model regime. To fold to the observed wavelengths, the slab could be only ~100 times more viscous than the surrounding mantle for a wide range of in-plane elastic strain, or ≥3 orders of magnitude more viscous if an elastic strain close to 0.05 is allowed. Partly because of the folding, the Wadati-Benioff zone progressively steepens at depths below 80 km as approaching Taiwan. The double-seismic zone is clearly mapped out within the slab in the depth range of 40–80 km throughout much of the subduction-collision zone. The DSZ, with a gap of 15–20 km, is stressed by the same horizontal compression that folds the slab.

Appendix A

[32] We follow the linear operator approach of *Flügge* [1975]. The bending stress and strain for a two-dimensional layer are related by the linear operators:

$$P_l(\sigma) = Q_l(\varepsilon), \tag{A1}$$

where subscript l denotes the operators for layer. Without introducing material properties, the balance between the bending moment, horizontal compression per unit length perpendicular to the direction of compression N, and vertical loading q leads to

$$\frac{h^3}{12} Q_l\left(\frac{\partial^4 w}{\partial x^4}\right) + P_l\left(N\frac{\partial^2 w}{\partial x^2}\right) = P_l(q), \tag{A2}$$

where w is the vertical deflection of the layer, h the thickness of the layer, and x measures horizontal distance in N-parallel direction. For a Maxwell material that responds instantaneously to external stresses followed by a viscous deformation, the contributions from the elastic and viscous parts are summed on strain rate:

$$\dot{\varepsilon} = \frac{\dot{\sigma}}{E_l^*} + \frac{\sigma}{4\mu_l}. \tag{A3}$$

Here each contribution is for a thin plate, and $E_l^* = E_l/(1 - \nu^2)$ with E_l the Young's modulus of the layer, and μ_l the viscosity of the layer. With these, the operators are defined as

$$P_l = 1 + \tau_l \frac{\partial}{\partial t}, \quad Q_l = 4\mu_l \frac{\partial}{\partial t}, \tag{A4}$$

where $\tau_l = 4\mu_l/E_l^*$ is the relaxation time of the Maxwell material. Equation (A2) becomes

$$D_v \frac{\partial}{\partial t}\frac{\partial^4 w}{\partial x^4} + N\left(1 + \tau_l \frac{\partial}{\partial t}\right)\frac{\partial^2 w}{\partial x^2} = \left(1 + \tau_l \frac{\partial}{\partial t}\right) q. \tag{A5}$$

This is the governing equation for bending of a Maxwell layer under transverse loading q and in-plane compression N; $D_v = \mu_l h^3/3$ is the flexural rigidity of a viscous plate.

Equation (A5) reduces to bending of an elastic plate as $\mu_l \rightarrow \infty$ and $\tau_l \rightarrow \infty$:

$$D_e \cdot \frac{\partial^4 w}{\partial x^4} + N \cdot \frac{\partial^2 w}{\partial x^2} = q, \tag{A6}$$

where $D_e = E_l^* h^3/12$ is the flexural rigidity of an elastic plate. Equation (A5) reduces to viscous plate bending as $E_l^* \rightarrow \infty$ and $\tau_l \rightarrow 0$:

$$D_v \cdot \frac{\partial^4 \dot{w}}{\partial x^4} + N \cdot \frac{\partial^2 w}{\partial x^2} = q. \tag{A7}$$

[33] Because external loading is passive in a folding problem, the medium operators link q with deflection w:

$$P_m(q) = Q_m(w). \tag{A8}$$

Assume the deflection w has the form of $w(x, t) = A(t)\sin(kx)$,

$$P_m = 1, \quad Q_m = -4k\mu_m \frac{\partial}{\partial t} \tag{A9}$$

for viscous medium, where μ_m is the viscosity of the medium. Equation (A9) implies that the resistance is proportional to the wavelength at which the layer is folded. Inserting (A8) and (A9) into (A5) to eliminate q, we obtain

$$D_v \frac{\partial w''''}{\partial t} + Nw'' + \tau_l N \frac{\partial w''}{\partial t} = -4k\mu_m \frac{\partial w}{\partial t} - 4k\mu_m \tau_l \frac{\partial^2 w}{\partial t^2}. \tag{A10}$$

The characteristic equation for the solution of the form of $A(t)\sin(kx)$ is

$$4\mu_m \tau_l \frac{\partial^2 A}{\partial t^2} - \left[\tau_l Nk - D_v k^3 - 4\mu_m\right] \frac{\partial A}{\partial t} - NKA = 0, \tag{A11}$$

and $A(t)$ is composed of two terms: $\exp(\omega_1 t)$ and $\exp(\omega_2 t)$ where

$$\omega_{1,2}\tau_l = \frac{\gamma}{8}\left[-b \pm \sqrt{b^2 + c}\right], \tag{A12}$$

where

$$b = \frac{\overline{k}^3}{3} - 4\varepsilon_N \overline{k} + \frac{4}{\gamma}, c = 64\varepsilon_N \frac{\overline{k}}{\gamma}, \tag{A13}$$

and $\gamma = \mu_l/\mu_m$. The normalized wave number $\overline{k} = 2\pi/(\lambda/h)$, and ε_N is defined as

$$\varepsilon_N = \frac{N/h}{E_l^*}, \tag{A14}$$

which approximates the in-plane elastic strain or the membrane strain due to lateral compression. The amplification functions $\omega_1 > 0$ which promotes instability, and $\omega_2 < 0$ which stabilizes perturbations, but the total amplification rate is always greater than zero. The amplification ω_1 can be plotted as a function of normalized wavelength and the wavelength for the dominant member of folding λ_d can be found numerically. The result is consistent with that of *Schmalholz and Podladchikov* [1999].

[34] For the case of an elastic layer embedded in a viscous medium, we start with equation (A6) to derive the dominant wavelength:

$$\frac{\lambda_d}{h} = \pi\left[\frac{1}{\varepsilon_N}\right]^{1/2} \tag{A15}$$

The instability occurs when $\lambda > (1/3)^{1/2}\lambda_d$. For a viscous layer folding in a viscous medium, λ_d can also be expressed analytically:

$$\frac{\lambda_d}{h} = 2\pi\left[\frac{\gamma}{6}\right]^{1/3}. \tag{A16}$$

The derivation of equations (A15) and (A16) is given by *Biot* [1961].

[35] **Acknowledgments.** We thank Tetsuzo Seno, Jer-Ming Chiu, and Geoffrey Abers for their critical reviews. Comments by Stefan Schmalholz, Serge Lallemand, Jean-Claude Sibuet, and Yves Font are appreciated. Discussion with Wen-Tzong Liang led to the important analysis into the CWB time tagging problem. The work is supported by the National Science Council of Taiwan, Republic of China, under grant NSC 94-2116-M-001-015.

References

Abers, G. A. (1992), Relationship between shallow and intermediate depth seismicity in the eastern Aleutian subduction zone, *Geophys. Res. Lett.*, *19*, 2019–2022.

Bergman, E. A., and S. C. Solomon (1990), Earthquake swarms on the Mid-Atlantic Ridge: Products of magmatism or extensional tectonics?, *J. Geophys. Res.*, *95*, 4943–4965.

Bevis, M. (1988), Seismic slip and down-dip strain rates in Wadati-Benioff zones, *Sciences*, *240*, 1317–1319.

Billen, M. I., M. Gurnis, and M. Simons (2003), Multiscale dynamics of the Tonga-Kermadec subduction zone, *Geophys. J. Int.*, *153*, 359–388.

Biot, M. A. (1961), Theory of folding of stratified viscoelastic media and its implications in tectonics and orogenesis, *Geol. Soc. Am. Bull.*, *72*, 1595–1620.

Burbach, G. V., and C. Frohlich (1986), Intermediate and deep seismicity and lateral structure of subducted lithosphere in the circum-Pacific region, *Rev. Geophys.*, *24*, 833–874.

Caldwell, J. G., W. F. Haxby, D. E. Karig, and D. L. Turcotte (1976), On the applicability of a universal elastic trench profile, *Earth Planet. Sci. Lett.*, *31*, 239–246.

Chen, W. P., and M. R. Brudzinski (2001), Evidence for a large-scale remnant of subducted lithosphere beneath Fiji, *Science*, *292*, 2475–2479.

Chen, Y. L. (1995), A study of 3-D velocity structure of the crust and the subduction zone in the Taiwan region (in Chinese), Master thesis, 172 pp., Natl. Cent. Univ., Jhongli City, Taiwan.

Chiao, L. Y. (1993), Strain segmentation and lateral membrane deformation rate of the subducted Ryukyu slab, *Island Arc*, *2*, 94–103.

Chiao, L. Y., H. Kao, S. Lallemand, and C. S. Liu (2001), An alternative interpretation for slip vector residuals of subduction interface earthquakes: A case study in the westernmost Ryukyu slab, *Tectonophysics*, *333*, 123–134.

Chiu, J.-M., B. L. Isacks, and R. K. Cardwell (1991), 3-D configuration of subducted lithosphere in the western Pacific, *Geophys. J. Int.*, *106*, 99–111.

Christensen, U. R. (1989), Mantle rheology, constitution and convection, in *Mantle Convection: Plate Tectonics and Global Dynamics*, *Fluid Mech. Astrophys. Geophys.*, vol. 4, edited by W. R. Peltier, pp. 595–655, Gordon and Breach, New York.

Cochran, J. R. (1979), An analysis of isostasy in the world's oceans: 2. Mid-ocean ridge crests, *J. Geophys. Res.*, *84*, 4713–4729.

Deschamps, A., S. E. Lallemand, and J.-Y. Collot (1998), A detailed study of the Gagua ridge: A fracture zone uplifted during a plate reorganization in the mid-Eocene, *Mar. Geophys. Res.*, *20*, 403–423.

Deschamps, A., P. Monié, S. Lallemand, S. K. Hsu, and K. Y. Yeh (2000), Evidence for early Cretaceous curst trapped in the Philippine Sea plate, *Earth Planet. Sci. Lett.*, *179*, 503–516.

Dziewonski, A. M., T.-A. Chou, and J. H. Woodhouse (1981), Determination of earthquake source parameters from waveform data for studies of global and regional seismicity, *J. Geophys. Res.*, *86*, 2825–2852.

Engdahl, E. R., R. D. van der Hilst, and R. P. Buland (1998), Global teleseismic earthquake relocation with improved travel times and procedures for depth determination, *Bull. Seismol. Soc. Am.*, *88*, 722–734.

Escartin, J., G. Hirth, and B. Evans (1997), Effects of serpentinization on the lithospheric strength and the style of normal faulting at slow-spreading ridges, *Earth Planet. Sci. Lett.*, *151*, 181–189.

Flügge, W. (1975), *Viscoelasticity*, 194 pp., Springer, New York.

Font, Y., S. Lallemand, and J. Angelier (1999), Etude de la transition entre l'orogene actif de Taiwan et la subduction des Ryukyu apports de la sismicite, *Bull. Soc. Geol. Fr.*, *170*(3), 271–283.

Font, Y., C. S. Liu, P. Schnurle, and S. Lallemand (2001), Constraints on backstop geometry of the southwest Ryukyu subduction based on reflection seismic data, *Tectonophysics*, *333*, 135–158.

Gudmundsson, O., and M. Sambridge (1998), A regionalized upper mantle (RUM) seismic model, *J. Geophys. Res.*, *103*, 7121–7136.

Hasegawa, A., N. Umino, and A. Takagi (1978), Double planed structure of the deep seismic zone in northeastern Japan arc, *Tectonophysics*, *47*, 43–58.

Hasegawa, A., S. Horiuchi, and N. Umino (1994), Seismic structure of the northeastern Japan convergent plate margin: A synthesis, *J. Geophys. Res.*, *99*, 22,295–22,311.

Hirth, G., J. Escartin, and J. Lin (1998), The rheology of the lower oceanic crust: Implications for lithospheric deformation at mid-ocean ridges, in *Faulting and Magmatism at Mid-ocean Ridges*, *Geophys. Monogr. Ser.*, vol. 106, edited by W. R. Buck et al., pp. 291–303, AGU, Washington, D. C.

Houseman, G. A., and D. Gubbins (1997), Deformation of subducted oceanic lithosphere, *Geophys. J. Int.*, *131*, 535–551.

Hsu, S. K. (2001), Subduction/collision complexities in the Taiwan-Ryukyu junction area: Tectonics of the northwestern corner of the Philippine Sea plate, *Terr. Atmos. Oceanic Sci.*, suppl. issue, 209–230.

Kao, H., and R. J. Rau (1999), Detailed structure of the subducted Philippine Sea plate beneath northeast Taiwan: A new type of double seismic zone, *J. Geophys. Res.*, *104*, 1015–1033.

Kao, H., S. J. Shen, and K. F. Ma (1998), Transition from oblique subduction to collision: Earthquakes in the southernmost Ryukyu arc-Taiwan region, *J. Geophys. Res.*, *103*, 7211–7229.

Kawakatsu, H. (1986), Double seismic zones: Kinematics, *J. Geophys. Res.*, *91*, 4811–4825.

Kim, K. H., J. M. Chiu, J. Pujol, K. C. Chen, B. S. Huang, Y. H. Yeh, and P. Shen (2005), Three-dimensional V_P and V_S structural models associated with the active subduction and collision tectonics in the Taiwan region, *Geophys. J. Int.*, *162*, 204–220, doi:10.1111/j.1365-246X.2005.02657.x.

King, S. (2001), Subduction zones: Observations and geodynamic models, *Phys. Earth Planet. Inter.*, *127*, 9–24.

Kirby, S. (1995), Intraslab earthquakes and phase changes in subducting lithosphere, *Rev. Geophys.*, *33*, 287–297.

Kirby, S. H., E. R. Engdahl, and R. Denlinger (1996), Instraslab earthquakes and arc volcanism: Dual physical expressions of crustal and uppermost mantle metamorphism in subduction slabs, in *Subduction: Top to Bottom, Geophys. Monogr. Ser.*, vol. 96, edited by G. E. Bebout et al., pp. 195–214, AGU, Washington, D. C.

Kissling, E., W. L. Ellsworth, and U. Kradolfer (1994), Initial reference models in local earthquake tomography, *J. Geophys. Res.*, *99*, 19,635–19,646.

Kohlstedt, D. L., B. Evans, and S. J. Mackwell (1995), Strength of the lithosphere: Constraints imposed by laboratory experiments, *J. Geophys. Res.*, *100*, 17,587–17,602.

Kuo, B. Y., D. F. Forsyth, and E. M. Parmentier (1986), Flexure and thickening of the lithosphere at the East Pacific Rise, *Geophys. Res. Lett.*, *13*, 681–684.

Liang, W. T., Y. H. Liu, and H. Kao (2004), Source parameters of regional earthquakes in Taiwan: January–December, 2002, *Terr. Atmos. Oceanic Sci.*, *15*, 727–741.

Lin, J. Y., S. K. Hsu, and J. C. Sibuet (2004), Melting features along the western Ryukyu slab edge (northeast Taiwan): Tomographic evidence, *J. Geophys. Res.*, *109*, B12402, doi:10.1029/2004JB003260.

Lin, S. C., L. Y. Chiao, and B. Y. Kuo (2002), Dynamic interaction of cold anomalies with the mid-ocean ridge flow field and its implications for the Australian–Antarctic Discordance, *Earth Planet. Sci. Lett.*, *203*, 925–935.

Ma, K. F., J. H. Wang, and D. Zhao (1996), Three-dimensional seismic velocity structure of the crust and uppermost mantle beneath Taiwan, *J. Phys. Earth*, *44*, 85–105.

Mallet, J. L. (1989), Discrete smooth interpolation, *Trans. Graph.*, *8*(2), 121–144.

Mallet, J. L. (2002), *Geomodeling*, 624 pp., Oxford Univ. Press, New York.

McGuire, J. J., and D. A. Wiens (1995), A double seismic zone in New Britain and the morphology of the Solomon plate at intermediate depths, *Geophys. Res. Lett.*, *22*, 1965–1968.

Pavlis, G. L., and J. R. Booker (1980), The mixed discrete-continuous inverse problem; application to the simultaneous determination of earthquake hypocenters and velocity structure, *J. Geophys. Res.*, *85*, 4801–4810.

Peacock, S. M. (2001), Are the lower planes of double seismic zones caused by serpentine dehydration in subducting oceanic lithosphere, *Geology*, *29*, 299–302.

Peacock, S. M. (2004), Thermal structure and metamorphic evolution of subducting slabs, in Inside the subduction factory, in *Inside the Subduction Factory, Geophys. Monogr. Ser.*, vol. 138, edited by J. Eiler, pp. 7–22, AGU, Washington, D. C.

Peacock, S. M., and K. Wang (1999), Seismic consequences of warm versus cool subduction metamorphism: Examples from southwest and northeast Japan, *Science*, *286*, 937–939.

Pysklywec, R. N., J. X. Mitrovica, and M. Ishii (2003), Mantle avalanche as a driving force for tectonic reorganization in the southwest Pacific, *Earth Planet. Sci. Lett.*, *209*, 29–38.

Ranero, C. R., J. Phipps Morgan, K. Mcintosh, and C. Reichert (2003), Bending-related faulting and mantle serpentinization at the middle America trench, *Nature*, *425*, 367–373.

Rau, R. J., and F. T. Wu (1995), Tomographic imaging of lithospheric structure under Taiwan, *Earth Planet. Sci. Lett.*, *133*, 517–532.

Schmalholz, S. M., and Y. Podladchikov (1999), Buckling versus folding: Importance of viscoelasticity, *Geophys. Res. Lett.*, *26*, 2641–2644.

Schnurle, P., C. S. Liu, S. Lallemand, and D. Reed (1998), Structural insight into the south Ryukyu margin: Effect of the subducting Gagua ridge, *Tectonophysics*, *288*, 237–250.

Seno, T., and S. Maruyama (1984), Paleogeographic reconstruction and origin of the Philippine Sea, *Tectonophysics*, *102*, 53–84.

Seno, T., and Y. Yamanaka (1996), Double seismic zones, compressional deep trench-outer rise events, and superplumes, in *Subduction: Top to Bottom*, *Geophys. Monogr. Ser.*, vol. 96, edited by G. E. Bebout et al., pp. 347–355, AGU, Washington, D. C.

Seno, T., S. Stein, and A. E. Gripp (1993), A model for the motion of the Philippine Sea plate consistent with NUVEL-1 and geological data, *J. Geophys. Res.*, *98*, 17,941–17,948.

Sibuet, J. C., et al. (1998), Okinawa trough back-arc basin: Early tectonic and magmatic evolution, *J. Geophys. Res.*, *103*, 30,245–30,267.

van der Hilst, R., and T. Seno (1993), Effects of relative plate motion on the deep structure and penetration depth of slabs below the Izu-Bonin and Marian island arcs, *Earth Planet. Sci. Lett.*, *120*, 395–407.

Waldhauser, F., and W. L. Ellsworth (2000), A double-difference earthquake location algorithm: Method and application to the northern Hayward fault, *Bull. Seismol. Soc. Am.*, *90*, 1353–1368.

Wang, K., and G. C. Rogers (1994), An explanation for the double seismic layers north of the Mendocino triple junction, *Geophys. Res. Lett.*, *21*, 121–124.

Wang, K., S. L. Chung, S. Y. O'Reilly, S. S. Sun, R. Shinjo, and C. H. Chen (2004a), Geochemical constraints for the genesis of post-collisional magmatism and the geodynamic evolution of the northern Taiwan region, *J. Petrol.*, *45*, 975–1011.

Wang, T. K., S. F. Lin, C. S. Liu, and C. S. Wang (2004b), Crustal structure of the southernmost Ryukyu subduction zone: OBS, MCS and gravity modeling, *Geophys. J. Int.*, *157*, 147–163.

Watts, A. B. (1978), An analysis of isostasy in the world's oceans: 1. Hawaiian-Emperor seamount chain, *J. Geophys. Res.*, *83*, 5989–6004.

Wiens, D. A., and S. Stein (1984), Intraplate seismicity and stresses in young oceanic lithosphere, *J. Geophys. Res.*, *89*, 11,442–11,464.

Wolfe, C., G. M. Purdy, D. R. Toomey, and S. C. Solomon (1995), Microearthquake characteristics and crustal velocity structure at 29°N of the Mid-Atlantic Ridge: The architecture of a slow spreading segment, *J. Geophys. Res.*, *100*, 24,449–24,472.

Wu, F. T., C. S. Chang, and Y. M. Wu (2004), Precisely relocated hypocenters, focal mechanisms and active orogeny in central Taiwan, in *Aspects of the Tectonic Evolution of China*, edited by J. Malpas et al., *Geol. Soc. Spec. Publ.*, *226*, 333–354.

Yamaoka, K., Y. Fuako, and M. Kumazawa (1986), Spherical shell tectonics: Effects of sphericity and inextensibility on the geometry of the descending lithosphere, *Rev. Geophys.*, *24*, 27–55.

Yamasaki, T., and T. Seno (2003), Double seismic zone and dehydration embrittlement of the subducting slab, *J. Geophys. Res.*, *108*(B4), 2212, doi:10.1029/2002JB001918.

L.-Y. Chiao, Institute of Oceanography, National Taiwan University, No.1, Sec. 4, Roosevelt Road, Taipei, 106 Taiwan. (chiao@ntu.edu.tw)

H.-C. Chou, S.-H. Hung, and Y.-M. Wu, Institute of Geosciences, National Taiwan University, P.O. Box 13-318, No.1, Sec. 4, Roosevelt Road, Taipei, 106 Taiwan. (d92224001@ntu.edu.tw; drymwu@ntu.edu.tw)

B.-Y. Kuo, Institute of Earth Sciences, Academia Sinica, No.128, Sec. 2, Academia Road, Nankang, Taipei, 115 Taiwan. (byk@earth.sinica.edu.tw)

D. Zhao, Geodynamic Research Center, Ehime University, 2–5, Bunkyo-cho, Matsuyama, 790-8577 Japan. (zhao@sci.ehime-u.ac.jp)